

Strong-coupling analysis of large- N two-dimensional lattice chiral models

Massimo Campostrini, Paolo Rossi, and Ettore Vicari

Dipartimento di Fisica dell'Università and INFN, I-56126 Pisa, Italy

(Received 8 February 1995)

$N = \infty$ two-dimensional chiral models on the square and honeycomb lattices are investigated by a strong-coupling analysis. The strong-coupling expansion turns out to be predictive for the evaluation of continuum physical quantities, to the point of showing asymptotic scaling. Indeed in the strong-coupling region a quite large range of β values exists where the fundamental mass agrees, within about 5% on the square lattice and about 10% on the honeycomb lattice, with the continuum predictions in the energy scheme.

PACS number(s): 11.15.Ha, 11.15.Me, 11.15.Pg, 75.10.Hk

I. INTRODUCTION

Recent numerical studies of lattice two-dimensional $SU(N) \times SU(N)$ principal chiral models, with the standard nearest-neighbor interaction

$$S_L = -2N\beta \sum_{x,\mu} \text{Re Tr} [U(x)U^\dagger(x+\mu)], \quad \beta = \frac{1}{NT}, \quad (1)$$

have shown the existence of a scaling region, where continuum predictions for dimensionless ratios of physical quantities are substantially verified [1–3]. The scaling region begins at relatively small values of the correlation length well within the expected region of convergence of strong-coupling expansion. Moreover, by performing a variable change [4] from the temperature T to

$$T_E = \frac{8N}{N^2 - 1} E, \quad \beta_E = \frac{1}{NT_E}, \quad (2)$$

where E is the internal energy, one can find agreement in the whole scaling region between the measured mass scale and the asymptotic scaling prediction, within few percent [2].

As a matter of fact, this may be considered as evidence for asymptotic scaling within the strong-coupling regime, motivating a test of scaling and asymptotic scaling by strong-coupling computations. As a by-product, strong-coupling series can be analyzed to investigate the critical behavior of the $N = \infty$ theory, where Monte Carlo data seem to indicate the existence of a phase transition at finite β .

Reference [5] was devoted to a complete presentation of our strong-coupling calculations performed by means of the character expansion. We calculated strong-coupling series for several quantities on the square and honeycomb lattices. On the ordinary square lattice, we calculated the free energy up to $O(\beta^{18})$ and the fundamental Green's function

$$G(x) = \left\langle \frac{1}{N} \text{Re Tr} [U(x)U(0)^\dagger] \right\rangle \quad (3)$$

up to $O(\beta^{15})$. For chiral models on the honeycomb lattice, defined by the nearest-neighbor action, longer series

were obtained: the free energy up to $O(\beta^{26})$ and $G(x)$ up to $O(\beta^{20})$. Lattice chiral models on square and honeycomb lattices are expected to belong to the same class of universality with respect to the continuum limit. As we will see from the strong-coupling analysis, even at finite β large- N chiral models on the honeycomb lattices show a pattern very similar to that observed on the square lattice.

In this paper, which represents the logical continuation of Ref. [5], we analyze the $N = \infty$ strong-coupling series presented there and the results are compared with the continuum limit predictions and Monte Carlo simulations. The main result of our strong-coupling analysis of two-dimensional $N = \infty$ chiral models on the square and honeycomb lattices is the identification of a scaling region where known continuum results are reproduced with good accuracy, and asymptotic predictions are substantially satisfied in the energy scheme.

II. STRONG-COUPLING EVIDENCE OF A LARGE- N PHASE TRANSITION

Numerical simulations at large N of $SU(N)$ and $U(N)$ lattice chiral models show evidence of a phase transition at $N = \infty$. Indeed sharper and sharper peaks in the specific heat

$$C = \frac{1}{N} \frac{dE}{dT} \quad (4)$$

are observed with increasing N , suggesting a divergent large- N limit at a finite β [2]. By extrapolating to $N = \infty$ the positions of the specific heat peaks, we obtained a rather precise estimate of the critical coupling: $\beta_c = 0.3057(3)$. Details of our Monte Carlo simulations and their analysis can be found in Ref. [6].

In order to investigate the above issue, we analyze the $N = \infty$ strong-coupling series by employing the integral approximant technique [7–9], which is especially recommended in the case of a small critical exponent. The integral approximant method consists of representing the power series under study by the integral of a linear differential equation. In our analysis we considered the integral

approximants obtained from a first-order linear differential equation

$$Q_L(x)f'(x) + P_K(x)f(x) + R_J(x) = O(x^{L+K+J+2}), \quad (5)$$

where Q_L , P_K , and R_J are, respectively, L , K , and J order polynomials (we fix $Q_{L,0} = 1$). These approximants are singular at the zeros x_0 of $Q_L(x)$, and behave as

$$A(x)|x - x_0|^{-\gamma} + B(x), \quad (6)$$

where $A(x)$ and $B(x)$ are regular in the neighborhood of x_0 , and

$$\gamma = -\frac{P_K(x_0)}{Q'_L(x_0)}. \quad (7)$$

Given an M order series, L , K , and J must satisfy the condition $L + K + J + 2 \leq M$.

Let us analyze the $N = \infty$ strong-coupling series of the specific heat, which is even in β :

$$\begin{aligned} \beta^{-2}C = & 1 + 6x + 30x^2 + 266x^3 + 2160x^4 + 19932x^5 \\ & + 183638x^6 + 1754130x^7 + 16911192x^8 \\ & + O(x^9), \end{aligned} \quad (8)$$

where $x = \beta^2$. In Table I we report the first singularity in the real axis and the corresponding exponent for different values of L , K , and J . The results are quite stable, leading to a critical behavior of the specific heat typical of a second-order phase transition:

$$C \sim |\beta - \beta_c|^{-\alpha}. \quad (9)$$

From Table I we estimate

$$\begin{aligned} \beta_c &= 0.3058(3), \\ \alpha &= 0.23(3). \end{aligned} \quad (10)$$

TABLE I. Resummation of the strong-coupling series of the specific heat. We analyze the series of $\beta^{-2}C$ expressed in terms of β^2 [cf. Eq. (8)] for which $M = 8$. We report the first singularity in the real axis, $\beta_0 \equiv \sqrt{x_0}$, and the corresponding exponent versus L , K , and J .

L	K	J	β_0	γ
2	2	2	0.30598	0.252
2	3	1	0.30566	0.227
2	1	3	0.30586	0.245
2	0	4	0.30563	0.228
2	4	0	0.30569	0.228
3	2	1	0.30697	0.280
3	1	2	0.30591	0.250
3	3	0	0.30568	0.228
3	0	3	0.30619	0.277
4	1	1	0.30508	0.183
4	2	0	0.30475	0.166
4	0	2	0.30570	0.233
5	1	0	0.30562	0.222
5	0	1	0.30588	0.241
6	0	0	0.30564	0.225

The errors are just indicative. They are the variance of the results in Table I after discarding the two furthest values from the corresponding average; they should give an idea of the spread of the results coming from different approximants. Notice that the strong-coupling determination of β_c is in agreement with its estimate from numerical simulations at large N .

As a further check of the above resummation procedure, Fig. 1 compares, in the region $\beta < \beta_c$, $SU(N)$ and $U(N)$ Monte Carlo data of the specific heat at large N [$N = 21, 30$ for $SU(N)$ and $N = 15, 21$ for $U(N)$] with the determinations coming from the resummed and the plain strong-coupling series (8). We recall that $SU(N)$ and $U(N)$ models should have the same large- N limit. Monte Carlo data of C appear to approach, for growing N , the determination from the resummed strong-coupling series. As expected from simple considerations on the finite- N corrections to the $N = \infty$ strong-coupling series, $U(N)$ models converge faster than $SU(N)$ models to the $N = \infty$ limit in the strong-coupling region.

Monte Carlo data at large N seem to indicate that all physical quantities, such as the magnetic susceptibility $\chi \equiv \sum_x G(x)$ and the second-moment mass M_G^2 [$M_G \equiv 1/\xi_G$ and $\chi\xi_G^2 \equiv \frac{1}{4} \sum_x x^2 G(x)$], are well-behaved functions of the internal energy even at $N = \infty$ [2]. Therefore, as a consequence of the specific-heat divergence, χ and M_G^2 should have a singular behavior with respect to β . We indeed expect

$$\frac{d \ln \chi}{d\beta} \sim \frac{d \ln M_G^2}{d\beta} \sim |\beta - \beta_c|^{-\alpha} \quad (11)$$

in the neighborhood of β_c . Notice that a behavior such as Eq. (11) leads to a nonanalytical zero of the β function $\beta_L(T)$ at β_c ,

$$\beta_L(T) \sim |\beta - \beta_c|^\alpha, \quad (12)$$

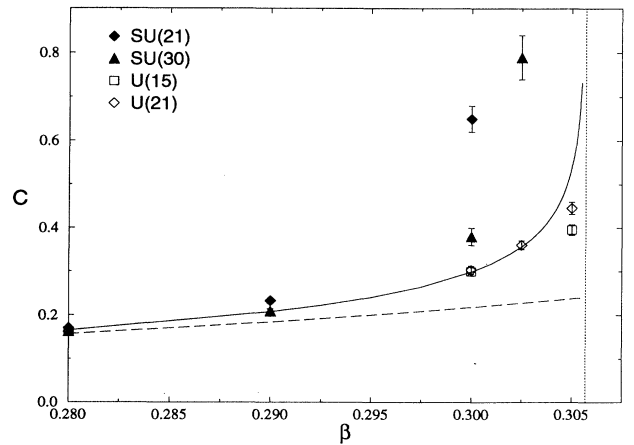


FIG. 1. Specific heat vs β . The dashed and solid lines represent the plain strong-coupling series and its resummation. The estimate of the critical β is indicated by vertical dotted lines. When error bars are not visible, they are smaller than the symbol size.

around β_c , explaining the observed behavior with respect to β of the large- N Monte Carlo data for the fundamental mass [2].

In order to check Eq. (11), we analyzed the corresponding strong-coupling series by a modified integral approx-

imant scheme forcing the approximant to have a singularity at $\beta \simeq 0.3058$, obtaining biased estimates of the exponent in Eq. (11). In this modified scheme the values of L , K , and J in Eq. (5) must be chosen according to the condition $L + K + J + 1 \leq M$. We analyze the series

$$\frac{d \ln \chi}{d\beta} = 4 + 8\beta + 28\beta^2 + 48\beta^3 + 204\beta^4 + 440\beta^5 + 1740\beta^6 + 3744\beta^7 + 15148\beta^8 + 35048\beta^9 + 140980\beta^{10} + 327600\beta^{11} + 1323612\beta^{12} + 3149112\beta^{13} + 12727908\beta^{14} + O(\beta^{15}), \quad (13)$$

and

$$\frac{d \ln(\beta M_G^2)}{d\beta} = -4 - 10\beta - 28\beta^2 - 74\beta^3 - 224\beta^4 - 598\beta^5 - 1936\beta^6 - 5282\beta^7 - 17560\beta^8 - 49170\beta^9 - 162144\beta^{10} - 464426\beta^{11} - 1549656\beta^{12} - 4459234\beta^{13} + O(\beta^{14}). \quad (14)$$

In Table II we report the range of the exponent variations when varying the zero in the interval 0.3055–0.3061. These results are quite consistent with the exponent α obtained in the analysis of the specific-heat strong-coupling series, supporting the relations (11) and therefore (12). Such resummations of the series (13) and (14) provide also improved $N = \infty$ strong-coupling estimates of χ and ξ_G . When performing an unbiased analysis of the series (13) and (14), that is, without forcing the approximants to have a zero at a fixed β , the singularity and the corresponding exponent turn out to be less stable; more terms in the series would be necessary to have a satisfactory analysis independent of that of the specific heat.

In Fig. 2 we compare our strong-coupling calculations of χ with Monte Carlo data of $SU(N)$ and $U(N)$ chiral models at large N . In the strong-coupling region the $SU(N)$ and $U(N)$ data appear clearly to approach the same $N \rightarrow \infty$ limit, which turns out to be very well reproduced by the improved strong-coupling estimate obtained by integrating the resummed series of $d \ln \chi / d\beta$ (using $L = 5$, $K = 4$, and $J = 4$; see Table II). As Monte Carlo data show, the large- N convergence around the transition point is much slower, especially in the weak-coupling domain.

TABLE II. Analysis of the series of $d \ln \chi / d\beta$ and $d \ln(\beta M_G^2) / d\beta$. For some set of L , K , and J we report the range of values of γ corresponding to the range of zero values 0.3055–0.3061.

	L	K	J	γ
$d \ln \chi / d\beta$	4	5	4	0.20–0.24
	4	4	5	0.28–0.31
	5	4	4	0.23–0.27
	5	5	3	0.22–0.26
	6	3	4	0.22–0.26
	6	4	3	0.23–0.27
$d \ln(\beta M_G^2) / d\beta$	4	4	4	0.23–0.26
	5	4	3	0.26–0.30
	5	3	4	0.07–0.12
	6	3	3	0.10–0.15

III. SCALING AND ASYMPTOTIC SCALING

In spite of the existence of a phase transition at $N = \infty$, Monte Carlo data at large N showed scaling and approximate asymptotic scaling (in the energy scheme) even for β smaller than the peak of the specific heat [2]. The stability of this pattern suggests an effective decoupling of the modes responsible for the phase transition from those determining the physical continuum limit, and therefore that evidence of scaling and asymptotic scaling could be provided by the large- N strong-coupling expansion.

The on-shell fundamental mass M can be extracted from the long-distance behavior of the correlation function in the fundamental channel $G(x)$ or from the imaginary pole of its Fourier transform. We considered two estimators of M , μ_s , and μ_d , defined from the long-distance behavior of wall-wall correlation functions constructed with $G(x)$, respectively, along the sides and the diago-

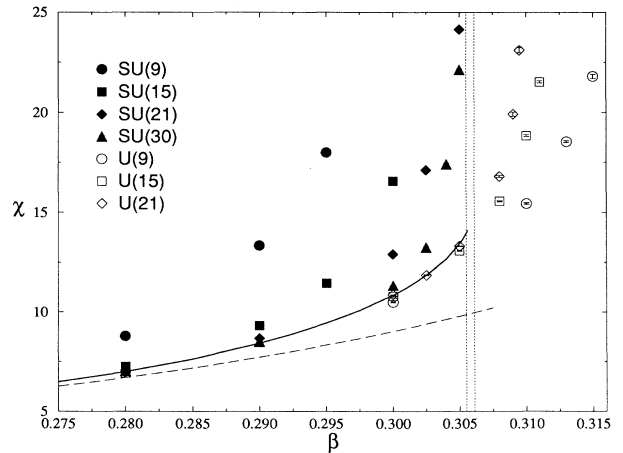


FIG. 2. Magnetic susceptibility vs β . The dashed and solid lines represent the plain strong-coupling series and the result coming from the resummation of the series (13), respectively. The estimate of the critical β is indicated by the vertical dotted lines.

nals of the lattice. An alternative mass M_G is defined from the inverse second moment of $G(x)$. Unlike the on-shell mass M , M_G is an off-shell quantity; it is related to the zero momentum of the Fourier transform of $G(x)$, indeed $\tilde{G}(p)^{-1} \sim M_G^2 + p^2$ at small momentum.

The quantities μ_s , μ_d , and M_G^2 allow one to perform tests of scaling based on rotational invariance at distances $d \gtrsim \xi \equiv 1/\mu_s$, checking $\mu_s/\mu_d \simeq 1$, and on the stability of dimensionless physical quantities, looking at the ratio μ_s/M_G . We should say that these tests concern the long-distance physics of chiral models.

Monte Carlo data at relatively large N showed that, within statistical errors of few per mille, the above scaling requirements are verified already at $\xi \simeq \xi_G \simeq 2$, well within the strong-coupling region. Indeed in $SU(N)$ lattice chiral models and for sufficiently large N , the position of the specific heat peak turns out to be quite stable with respect to the correlation length: $\xi_G^{\text{peak}} \simeq 2.8$ for $N \gtrsim 6$, leading also to the expectation that at the large- N critical point $\xi_G^{(c)} \simeq 2.8$ [2].

In Ref. [5] the strong-coupling series corresponding to the above-mentioned quantities have been calculated, in particular M_G^2 up to $O(\beta^{13})$, $M_s^2 \equiv 2(\cosh \mu_s - 1)$ up to $O(\beta^{11})$, and $M_d^2 \equiv 4(\cosh \mu_d/\sqrt{2} - 1)$ up to $O(\beta^{10})$.

In Fig. 3 we plot the ratio μ_s/μ_d vs the correlation length $\xi_G \equiv 1/M_G$ as obtained from our strong-coupling series. The $N = \infty$ strong-coupling curve confirms the large- N Monte Carlo result $\mu_s/\mu_d \simeq 1$ within a few per mille at $\xi \simeq 2$.

Figure 4 shows the ratio μ_s/M_G vs ξ_G . Notice the stability of the curve for a large region of values of ξ_G and the good agreement (well within 1%) with the continuum large- N value extrapolated by Monte Carlo data, which is $M/M_G = 0.991(1)$ [2].

In order to test asymptotic scaling we perform the variable change indicated in Eq. (2), evaluating the energy from its strong-coupling series. The two-loop renormalization group and a Bethe ansatz evaluation of the mass/ Λ -parameter ratio [10] lead to the following large- N asymptotic scaling prediction for the on-shell fundamental mass in the β_E scheme:

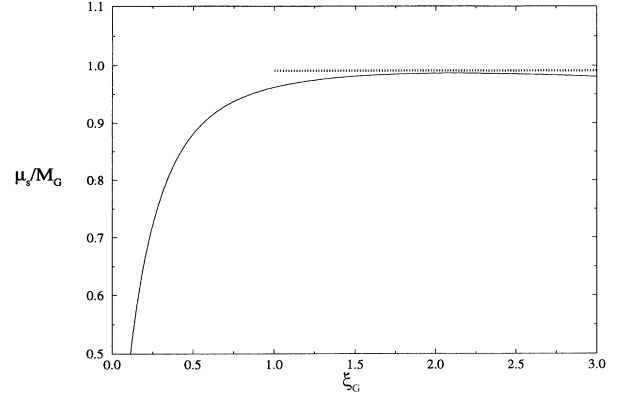


FIG. 4. μ_s/M_G vs $\xi_G \equiv 1/M_G$. The dashed lines represent the continuum limit result from Monte Carlo data.

$$\begin{aligned} M &\cong R_E \Lambda_{E,2l}(\beta_E), \\ R_E &= 16 \sqrt{\frac{\pi}{e}} \exp\left(\frac{\pi}{4}\right), \\ \Lambda_{E,2l}(\beta_E) &= \sqrt{8\pi\beta_E} \exp(-8\pi\beta_E), \\ \beta_E &= \frac{1}{8E}. \end{aligned} \quad (15)$$

In Fig. 5 the strong-coupling estimates of $\mu_s/\Lambda_{E,2l}$ and $M_G/\Lambda_{E,2l}$ are plotted vs β_E , for a region of coupling lengths $1.5 \lesssim \xi_G \lesssim 3$. (We recall that M_G differs from M by about 1% in the continuum limit.) The agreement with the exact continuum prediction is within about 5% in the whole region. Notice also that both curves go smoothly through the value of β_E corresponding to the specific-heat singularity β_c , which is $\beta_E^{(c)} \simeq 0.220$.

The strong-coupling curves in Fig. 5 were obtained from the plain series of the energy and respectively of M_s^2 and M_G^2 . In the case of M_G , we also determined $M_G/\Lambda_{E,2l}$ evaluating the energy and M_G^2 by integrating the resummed series, respectively, of the specific heat and of $d \ln \beta M_G^2/d\beta$. The resulting curve changes very little

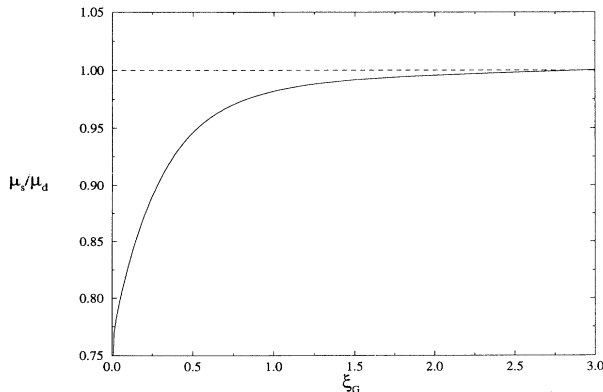


FIG. 3. μ_s/μ_d vs $\xi_G \equiv 1/M_G$.

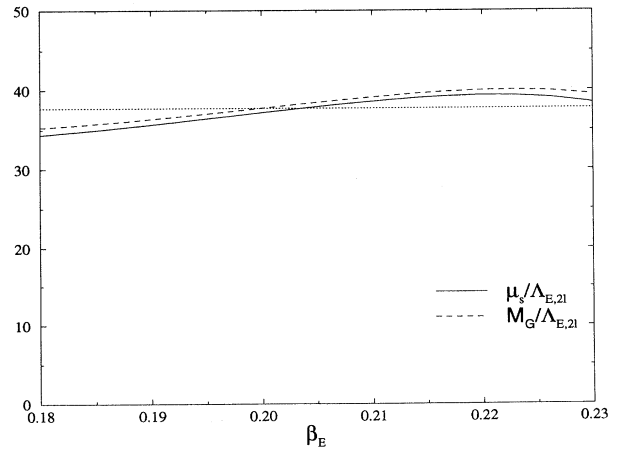


FIG. 5. Asymptotic scaling test by using strong-coupling estimates. The dotted line represents the exact result (15).

from that derived from the plain series; the difference between the two curves would not be visible in Fig. 5. This indicates once more that the change of variable $\beta \rightarrow \beta_E$ washes out the singularity in β when considering physical quantities.

IV. CHIRAL MODELS ON THE HONEYCOMB LATTICE

On the honeycomb lattice we consider the nearest-neighbor action, which can be written as a sum over all links of the honeycomb lattice:

$$S_h = -2N\beta \sum_{\text{links}} \text{Re Tr} [U_l U_r^\dagger], \quad U \in \text{SU}(N), \quad (16)$$

where l, r indicate the sites at the ends of each link. As on the square lattice, a lattice space a , which represents the lattice length unit, is defined to be the length of a link. The volume of an hexagon is $v_h = 3\sqrt{3}/2$. Straightforward calculations show that the correct continuum limit is obtained identifying

$$T = \frac{\sqrt{3}}{N\beta}. \quad (17)$$

A. Large- N phase transition

On the honeycomb lattice we have calculated the $N = \infty$ strong-coupling series of the specific heat, which is even in β , up to 26th order:

$$\begin{aligned} \beta^{-2}C = & 1 + 10x^2 + 90x^4 + 396x^5 + 728x^6 + 9120x^7 \\ & + 28186x^8 + 136800x^9 + 886116x^{10} \\ & + 3129380x^{11} + 18935800x^{12} + O(x^{13}), \end{aligned} \quad (18)$$

where $x = \beta^2$. The integral approximant analysis of the above series, whose results are reported in Table III, leads again to a second-order-type critical behavior with the following estimates of the critical β and exponent α :

TABLE III. Resummation of the 24th-order strong-coupling series of the specific heat for the honeycomb lattice. We analyze the series of $\beta^{-2}C$ expressed in terms of β^2 [cf. Eq. (18)] for which $M = 12$. We report the first singularity in the real axis, $\beta_0 \equiv \sqrt{x_0}$, and the corresponding exponent versus L, K , and J .

L	K	J	β_0	γ
3	4	3	0.43386	0.162
3	3	4	0.43389	0.165
4	3	3	0.43393	0.167
4	4	2	0.43398	0.171
4	2	4	0.43381	0.161
5	3	2	0.43387	0.163
5	2	3	0.43415	0.185
5	4	1	0.43397	0.171
5	1	4	0.43495	0.240
6	2	2	0.43312	0.101

$$\begin{aligned} \beta_c &= 0.4339(1), \\ \alpha &= 0.17(1). \end{aligned} \quad (19)$$

Notice that this estimate of the exponent α is very close to that of the square lattice. The uncertainty in both estimates cannot really exclude the fact that they are equal, which would be an indication of universality.

Also in this context we analyzed the strong-coupling series of the logarithmic derivative of the magnetic susceptibility χ and βM_G^2 by the modified integral approximant method which forces the existence of a zero at β_c . In Table IV we report the range of the exponent variations when varying the zero in the interval 0.4338–0.4340. As for the square lattice, the results in Table IV are consistent with a divergence characterized by the specific-heat exponent [cf. Eq. (11)], supporting the existence of a nonanalytical zero of the β function at β_c .

B. Scaling

On the hexagonal lattice the maximal violation of full rotational symmetry occurs for directions differing by a $\pi/6$ angle, and therefore, taking into account its discrete rotational symmetry, also by a $\pi/2$ angle. So a good test of rotation invariance is provided by the ratio between masses extracted from the long-distance behaviors of a couple of orthogonal wall-wall correlation functions constructed with $G(x)$.

In Ref. [5] we defined two orthogonal wall-wall correlation functions $G_1^{(w)}(x)$ and $G_2^{(w)}(x)$, with the corresponding masses μ_1 and μ_2 , which should both reproduce the on-shell fundamental mass M in the continuum limit. In order to extract μ_1 and μ_2 we evaluated the $O(\beta^{18})$ series of $\exp(-3\mu_1/2)$ and the $O(\beta^{17})$ series of $\exp(-\sqrt{3}\mu_2/2)$.

Figure 6 shows the ratio μ_1/μ_2 vs $\xi_G \equiv 1/M_G$. As expected from the better rotational symmetry of the honeycomb lattice, rotation invariance is set earlier than for the square lattice: Already at a correlation length $\xi_G \simeq 0.5$ $\mu_1/\mu_2 \simeq 1$ within 1%.

In Fig. 7 we plot the ratio μ_1/M_G vs ξ_G . The approach

TABLE IV. Analysis of the series of $d \ln \chi / d\beta$ (19th order) and $d \ln \beta M_G^2 / d\beta$ (18th order) for the honeycomb lattice. For some set of L, K , and J we report the range of values of γ corresponding to the range of zero values 0.4338–0.4340.

	L	K	J	γ
$d \ln \chi / d\beta$	6	6	6	0.15–0.16
	6	7	5	0.14–0.15
	6	5	7	0.14–0.15
	7	5	6	0.15–0.16
	7	6	5	0.30–0.30
	8	5	5	0.15–0.16
$d \ln(\beta M_G^2) / d\beta$	6	6	5	0.21–0.22
	6	5	6	0.22–0.23
	7	5	5	0.21–0.22
	8	4	5	0.17–0.18
	8	5	4	0.22–0.24

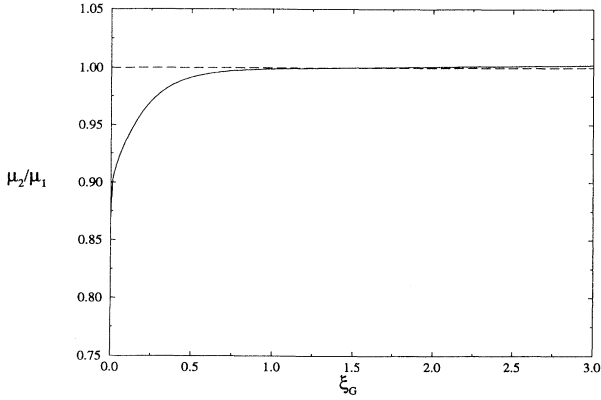


FIG. 6. μ_2/μ_1 vs $\xi_G \equiv 1/M_G$ for the honeycomb lattice.

to the continuum limit value seems to be substantially equivalent to that observed on the square lattice, but then for $\xi_G \gtrsim 1.5$ the curve becomes unstable. Such an instability should be cured by an extension of the series.

C. Asymptotic scaling

The asymptotic scaling test is again best performed in the energy scheme. This requires weak-coupling calculations, which present some subtleties on the honeycomb lattice. This is essentially due to the fact that, unlike square and triangular lattices, lattice sites are not characterized by a group of translations. Details on our weak-coupling calculations are given in the Appendix.

We calculated the internal energy (per link) up to two loops, finding

$$E = \frac{N^2 - 1}{N} \frac{T}{6\sqrt{3}} \left[1 + \frac{N^2 - 2}{N} \frac{T}{24\sqrt{3}} + O(T^2) \right]. \quad (20)$$

The energy scheme consists in defining a new temperature T_E proportional to the energy

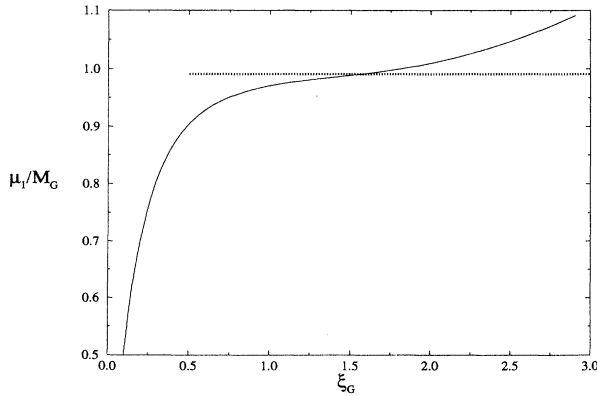


FIG. 7. μ_1/M_G vs $\xi_G \equiv 1/M_G$ for the honeycomb lattice. The dashed lines represent the continuum limit result from Monte Carlo data.

$$T_E = \frac{6\sqrt{3}N}{N^2 - 1} E, \quad \beta_E = \frac{1}{NT_E}. \quad (21)$$

The other important ingredient is the mass/ Λ -parameter ratio in the honeycomb lattice regularization, which requires the calculation of the ratio between the Λ parameter of the modified minimal subtraction ($\overline{\text{MS}}$) renormalization scheme $\Lambda_{\overline{\text{MS}}}$ and that of the honeycomb lattice regularization Λ_h , given that the (on-shell) mass/ Λ -parameter ratio in the $\overline{\text{MS}}$ scheme is known [10].

From a one-loop calculation we obtained

$$\frac{\Lambda_{\overline{\text{MS}}}}{\Lambda_h} = 4 \exp\left(\frac{N^2 - 2}{N^2} \frac{2\pi}{3\sqrt{3}}\right). \quad (22)$$

The ratio between $\Lambda_{h,E}$, the Λ parameter of the energy scheme, and Λ_h is easily obtained from the two-loop term of the internal energy:

$$\frac{\Lambda_h}{\Lambda_{h,E}} = \exp\left(-\frac{N^2 - 2}{N^2} \frac{\pi}{3\sqrt{3}}\right). \quad (23)$$

Then the $N = \infty$ asymptotic scaling prediction in the energy scheme is

$$\begin{aligned} M &\simeq R_{h,E} \Lambda_{E,2l}(\beta_E), \\ R_{h,E} &= 8\sqrt{\frac{2\pi}{e}} \exp\left(\frac{\pi}{3\sqrt{3}}\right), \\ \Lambda_{E,2l}(\beta_E) &= \sqrt{8\pi\beta_E} \exp(-8\pi\beta_E), \\ \beta_E &= \frac{1}{6\sqrt{3}E}. \end{aligned} \quad (24)$$

Figure 8 shows the ratios $\mu_1/\Lambda_{E,2l}$ and $M_G/\Lambda_{E,2l}$ vs β_E (corresponding to correlation lengths $1 \lesssim \xi_G \lesssim 2.5$), as obtained from the corresponding strong-coupling series. Again there is good agreement with the continuum prediction, especially in the region corresponding to correlation length $\xi_G \gtrsim 2$, where the agreement is within

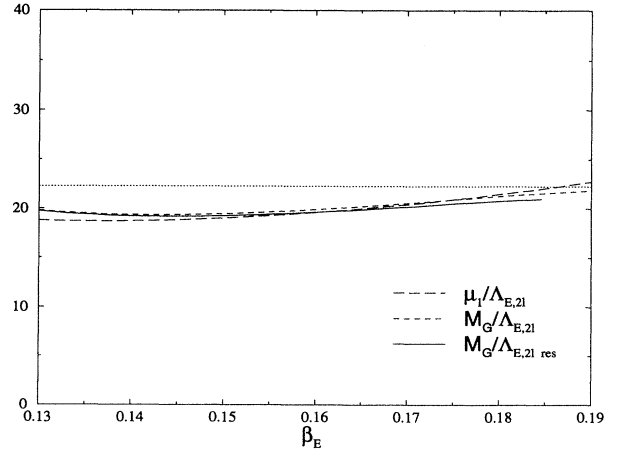


FIG. 8. Asymptotic scaling test for the honeycomb lattice by using strong-coupling estimates. The dotted line represents the exact result (24). The solid line corresponding to the ratio $M_G/\Lambda_{h,E}$ was constructed by resumming the involved strong-coupling series.

10%. The curve corresponding to M_G is more stable, and it changes little when calculated resumming the involved series.

APPENDIX: WEAK COUPLING EXPANSION ON THE HONEYCOMB LATTICE

On the honeycomb lattice the sites cannot be associated with a group of translation. This causes a few subtleties in the analysis of models on such a lattice.

The sites \vec{x} of a finite periodic hexagonal lattice can be represented in Cartesian coordinates by

$$\begin{aligned}\vec{x}(l_1, l_2, l_3) &= l_1 \vec{\eta}_1 + l_2 \vec{\eta}_2 + l_3 \left(\frac{1}{2}, 0\right), \\ l_1 &= 1, \dots, L_1, \quad l_2 = 1, \dots, L_2, \quad l_3 = -1, 1, \\ \vec{\eta}_1 &= \left(\frac{3}{2}, \frac{\sqrt{3}}{2}\right), \quad \vec{\eta}_2 = (0, \sqrt{3}).\end{aligned}\quad (\text{A1})$$

We set $a = 1$, where the lattice space a is the length of a link. The total number of hexagons on the lattice is $L_1 L_2$, while the sites are $2L_1 L_2$. The coordinate l_3 can be interpreted as the parity of the corresponding lattice site: Sites with the same parity are connected by an even number of links.

Notice that each of the two sublattices identified by $\vec{x}_-(l_1, l_2) \equiv \vec{x}(l_1, l_2, -1)$ and $\vec{x}_+(l_1, l_2) \equiv \vec{x}(l_1, l_2, 1)$ forms a triangular lattice. Each link of the honeycomb lattice connects sites belonging to different sublattices. Triangular lattices have a more symmetric structure, in that their sites are characterized by a group of translations. It is then convenient to rewrite a field $\phi(\vec{x}) \equiv \phi(l_1, l_2, l_3)$ in terms of two new fields $\phi_-(\vec{x}_-) \equiv \phi(\vec{x}_-)$ and $\phi_+(\vec{x}_+) \equiv \phi(\vec{x}_+)$ defined, respectively, on the sublattices \vec{x}_- and \vec{x}_+ . A finite lattice Fourier transform can be consistently defined as

$$\begin{aligned}\phi_{\pm}(\vec{p}) &= v_h \sum_{\vec{x}_{\pm}} e^{i\vec{p}\cdot\vec{x}_{\pm}} \phi_{\pm}(\vec{x}_{\pm}), \\ \phi_{\pm}(\vec{x}_{\pm}) &= \frac{1}{v_h L_1 L_2} \sum_{\vec{p}} e^{-i\vec{p}\cdot\vec{x}_{\pm}} \phi_{\pm}(\vec{p}),\end{aligned}\quad (\text{A2})$$

where $v_h = 3\sqrt{3}/2$ is the volume of an hexagon, and the set of momenta is

$$\begin{aligned}\vec{p} &= \frac{2\pi}{L_1} m_1 \vec{\rho}_1 + \frac{2\pi}{L_2} m_2 \vec{\rho}_2, \\ m_1 &= 1, \dots, L_1, \quad m_2 = 1, \dots, L_2, \\ \vec{\rho}_1 &= \left(\frac{2}{3}, 0\right), \quad \vec{\rho}_2 = \left(-\frac{1}{3}, \frac{1}{\sqrt{3}}\right).\end{aligned}\quad (\text{A3})$$

Notice that

$$\vec{p} \cdot \vec{x} = \frac{2\pi}{L_1} l_1 m_1 + \frac{2\pi}{L_2} l_2 m_2 + l_3 \frac{p_1}{2}.\quad (\text{A4})$$

To begin with, let us discuss the simple Gaussian models on the honeycomb lattice, whose action can be written as

$$S_G = \frac{\kappa}{2} \sum_{\text{links}} [\phi(x_l) - \phi(x_r)]^2,\quad (\text{A5})$$

where x_l, x_r indicate the sites at the ends of each link. Rewriting the field $\phi(x)$ in terms of two fields $\phi_-(x_-)$ and $\phi_+(x_+)$ as described above, and performing the Fourier transform (A2) we obtain

$$\begin{aligned}S_G &= \frac{\kappa}{\sqrt{3} v_h L_1 L_2} \sum_p [\phi_-(-p)\phi_-(p) + \phi_+(-p)\phi_+(p) \\ &\quad - \phi_-(-p)\phi_+(p)H(-p) - \phi_+(-p)\phi_-(p)H(p)],\end{aligned}\quad (\text{A6})$$

where

$$H(p) = e^{-ip_1} \frac{1}{3} \left(1 + 2e^{i\frac{3p_1}{2}} \cos \frac{\sqrt{3}p_2}{2} \right).\quad (\text{A7})$$

From (A6) we derive the propagators

$$\begin{aligned}\langle \phi_-(k)\phi_-(q) \rangle &= \langle \phi_+(k)\phi_+(q) \rangle = v_h \frac{\sqrt{3}}{\kappa} \frac{1}{\Delta(k)} \delta_{k+q,0}, \\ \langle \phi_+(k)\phi_-(q) \rangle &= v_h \frac{\sqrt{3}H(k)}{\kappa \Delta(k)} \delta_{k+q,0},\end{aligned}\quad (\text{A8})$$

where

$$\Delta(k) = \frac{8}{9} \left[2 - \cos \frac{\sqrt{3}}{2} k_2 \left(\cos \frac{3}{2} k_1 + \cos \frac{\sqrt{3}}{2} k_2 \right) \right].\quad (\text{A9})$$

When x_+ and x_- are the ends of the same link, i.e., $|x_+ - x_-| = 1$, one can easily prove that

$$\langle \phi_+(x_+)\phi_-(x_-) \rangle - \langle \phi_-(x_-)\phi_-(x_-) \rangle = -\frac{1}{3\kappa}.\quad (\text{A10})$$

The nearest-neighbor action of chiral models on the honeycomb lattice is

$$S_h = -\frac{\sqrt{3}}{T} \sum_{\text{links}} 2\text{Re Tr}[U_l U_r^\dagger], \quad U \in \text{SU}(N),\quad (\text{A11})$$

where l, r indicate the sites at the ends of each link. The perturbative expansion is performed by setting

$$U = e^{iA}, \quad A = \sum_a T_a A_a\quad (\text{A12})$$

[T_a are the generators of the $\text{SU}(N)$ group and A_a are $N^2 - 1$ real fields], and expanding U in powers of A . The action S_h becomes

$$\begin{aligned}S_h &= \frac{\sqrt{3}}{T} \sum_{\text{links}} \left[\text{Tr}(A_l - A_r)^2 + \frac{1}{4} \text{Tr}(A_l^2 - A_r^2)^2 \right. \\ &\quad \left. - \frac{1}{3} \text{Tr}(A_l - A_r)(A_l^3 - A_r^3) + O(A^6) \right].\end{aligned}\quad (\text{A13})$$

The change of variables (A12) requires the introduction of an additional term in the action

$$S_m = \frac{N}{12} \sum_{\text{sites}} \text{Tr} A_i^2 + O(A^4).\quad (\text{A14})$$

Then following the recipe illustrated in the Gaussian ex-

ample, we rewrite the field $A^\alpha(x_s)$ in terms of two new fields $A^\alpha(x_-)$ and $A^\alpha_+(x_+)$, whose propagators can easily be derived from those of the Gaussian models; cf. (A8). We are now ready to perform weak-coupling calculations.

Given the free energy per site,

$$F(\beta) = \frac{1}{n_s N^2} \ln \int \prod_x dU(x) \exp(-S_h), \quad (\text{A15})$$

where n_s is the number of sites, the internal energy (per link) can be obtained by

$$E = 1 - \frac{1}{3} \frac{dF(\beta)}{d\beta}. \quad (\text{A16})$$

The internal energy up to two loops is given by Eq. (20).

In order to evaluate the ratio between the Λ parameters of the $\overline{\text{MS}}$ renormalization scheme and the honeycomb-lattice regularization, we calculated the correlation function

$$G(T, x_+ - y_+) = \frac{1}{N} \langle \text{Re Tr}[U(x_+)U(y_+)^\dagger] \rangle. \quad (\text{A17})$$

In x space we obtained [neglecting $O(a)$ terms]

$$G(T, x, a) = 1 + \frac{N^2 - 1}{2N} T F(a/x) + O(T^2), \quad (\text{A18})$$

where

$$F(a/x) = \frac{1}{2\pi} \left(\ln \frac{a}{x} - \gamma_E - \ln 2 \right). \quad (\text{A19})$$

In p space

$$\begin{aligned} \tilde{G}(T, p, a) = & \frac{N^2 - 1}{2N} \frac{T}{p^2} \left[1 + \frac{N^2 - 2}{4N} T \left(D(ap) + \frac{1}{3\sqrt{3}} \right) \right. \\ & \left. + O(T^2) \right], \end{aligned} \quad (\text{A20})$$

where

$$D(ap) = \frac{1}{2\pi} (\ln ap - 2 \ln 2). \quad (\text{A21})$$

The above results required, in addition to the relation (A10), the calculation of the integrals

$$\begin{aligned} \int_{-\frac{2\pi}{3}}^{\frac{2\pi}{3}} \frac{dk_1}{2\pi} \int_{-\frac{\pi}{\sqrt{3}}}^{\frac{\pi}{\sqrt{3}}} \frac{dk_2}{2\pi} \frac{e^{ikx} - 1}{\Delta(k)} \\ = F(a/x) + O(a/x), \end{aligned} \quad (\text{A22})$$

$$\begin{aligned} \int_{-\frac{2\pi}{3}}^{\frac{2\pi}{3}} \frac{dk_1}{2\pi} \int_{-\frac{\pi}{\sqrt{3}}}^{\frac{\pi}{\sqrt{3}}} \frac{dk_2}{2\pi} \frac{\Delta(p) - \Delta(k) - \Delta(k+p)}{\Delta(k)\Delta(k+p)} \\ = 2D(ap) + O(ap), \end{aligned} \quad (\text{A23})$$

where the extremes of integration are chosen to cover the appropriate Brillouin zone, which can be determined from the finite lattice momenta (A3).

The next step consists in determining the renormalized functions $Z_t^{\overline{\text{MS}}}(T, a\mu)$ and $Z_U^{\overline{\text{MS}}}(T, a\mu)$ that satisfy the equations

$$\begin{aligned} G_R^{\overline{\text{MS}}}(t, x, \mu) &= Z_U^{\overline{\text{MS}}}(T, a\mu)^{-1} G(T, x, a), \\ T &= Z_t^{\overline{\text{MS}}}(T, a\mu) t, \end{aligned} \quad (\text{A24})$$

where t and $G_R^{\overline{\text{MS}}}(t, x, \mu)$ are, respectively, the coupling and the correlation function renormalized in the $\overline{\text{MS}}$ scheme. In the $\overline{\text{MS}}$ renormalization scheme we have [2]

$$\begin{aligned} G_R^{\overline{\text{MS}}}(t, x\mu = 2e^{-\gamma_E}) &= 1 + O(t^3), \\ \tilde{G}_R^{\overline{\text{MS}}}\left(t, \frac{p}{\mu} = 1\right) &= \frac{N^2 - 1}{2N} \frac{t}{p^2} [1 + O(t^2)]. \end{aligned} \quad (\text{A25})$$

Then by imposing Eqs. (A24) we obtain

$$Z_t^{\overline{\text{MS}}}(T, a\mu) = 1 + T \frac{N}{8\pi} (\ln a\mu + d) + O(T^2), \quad (\text{A26})$$

where

$$d = -2 \ln 2 - \frac{N^2 - 2}{N^2} \frac{2\pi}{3\sqrt{3}}. \quad (\text{A27})$$

The constant d determines the ratio $\Lambda_{\overline{\text{MS}}}/\Lambda_h$; indeed,

$$\frac{\Lambda_{\overline{\text{MS}}}}{\Lambda_h} = e^{-d} = 4 \exp\left(\frac{N^2 - 2}{N^2} \frac{2\pi}{3\sqrt{3}}\right). \quad (\text{A28})$$

For the interested reader we mention that Eqs. (A22) and (A23) may be derived from the exact result

$$\begin{aligned} \int_{-\frac{2\pi}{3}}^{\frac{2\pi}{3}} \frac{dk_1}{2\pi} \int_{-\frac{\pi}{\sqrt{3}}}^{\frac{\pi}{\sqrt{3}}} \frac{dk_2}{2\pi} \frac{1}{\Delta(k) + m^2 \left(1 + \frac{m^2}{8}\right)} \\ = \frac{1}{2\pi} \left(1 + \frac{3}{8}m^2\right)^{-3/2} \left(1 + \frac{1}{8}m^2\right)^{-1/2} \\ \times K \left[\left(1 + \frac{1}{4}m^2\right)^{1/2} \left(1 + \frac{3}{8}m^2\right)^{-3/2} \right. \\ \left. \times \left(1 + \frac{1}{8}m^2\right)^{-1/2} \right]. \end{aligned} \quad (\text{A29})$$

- [1] P. Rossi and E. Vicari, Phys. Rev. D **49**, 1621 (1994).
 [2] P. Rossi and E. Vicari, Phys. Rev. D **49**, 6072 (1994); **50**, 4718(E) (1994).
 [3] M. Camprostrini, P. Rossi, and E. Vicari, Phys. Rev. D

51, 958 (1995).

- [4] G. Parisi, in *High Energy Physics 1980*, Proceedings of the XXth Conference on High Energy Physics, Madison, Wisconsin, 1980, edited by L. Durand and L. G. Pon-

- drom, AIP Conf. Proc. No. 68 (AIP, New York, 1981).
- [5] M. Campostrini, P. Rossi, and E. Vicari, preceding paper, Phys. Rev. D **52**, 358 (1995).
 - [6] M. Campostrini, P. Rossi, and E. Vicari, following paper, Phys. Rev. D **52**, 395 (1995).
 - [7] A. J. Guttmann and G. S. Joyce, J. Phys. A **5**, L81 (1972).
 - [8] D. L. Hunter and G. A. Baker, Jr., Phys. Rev. B **49**, 3808 (1979).
 - [9] M. E. Fisher and H. Au-Yang, J. Phys. A **12**, 1677 (1979).
 - [10] J. Balog, S. Naik, F. Niedermayer, and P. Weisz, Phys. Rev. Lett. **69**, 873 (1992).